The effect of edge-stiffening and eccentric transverse prestresses in bridges

The Effects of Edge-Stiffening and Eccentric Transverse Prestress in Bridges

Influence du renforcement en bordure et de la précontrainte transversale excentrique dans les ponts

Die Wirkung von Randversteifung und extrentischer Quervorspannung in Brücken.

G. LITTLE
M. Sc., London

R. E. ROWE
M. A., A. M. I. C. E., London

Introduction

The development of the load distribution analysis for bridge decks subjected to concentrated loads [1, 2] has facilitated the calculation of the effects of abnormal indivisible loads on uniform bridge structures, i.e. structures which can be reduced to an equivalent quasi-slab. Often there is a deliberate reduction in the flexural stiffness at the footpaths either by a reduction in the structural depth, a change in the method of construction (e.g. unloaded filling material under the footpath slabs), or by the introduction of service ducts in the footpaths. Then the effective connexion of a parapet beam to the roadway is small compared with the connexion between the main road beams, and the modifying effects of the parapet beams, through their flexural and torsional stiffness, will not be significant. On the other hand the effective transverse stiffness of the roadway is sometimes maintained to the parapet beams. Then the effects of the stiffening beams at the edge should not be ignored. No theoretical analysis at present available covers this particular aspect of bridge design, though MASSONNET [3] has extended his distribution analysis [4] to allow for the effects of edge beams in which no torsional stiffness is present. This analysis should prove adequate in bridges consisting of longitudinal rolled steel joists with a reinforced concrete slab, the edge beams also being rolled steel joists of different section from the main longitudinal joists. However, in bridges in reinforced or prestressed concrete the torsional stiffness of the edge or parapet beam may be considerable.

Therefore an analysis has been obtained which includes the effect of torsion and, like the load distribution analyses already mentioned, covers the range from a no-torsion grillage to a full torsion slab. From this analysis it is possible to assess the effect of torsion in the edge beams at the design stage and hence it will be for the designer to use his judgment in deciding whether or not to include the torsional effects. If torsion is neglected the analysis yields results identical with those obtained by MASSONNET.

A further point of interest is that a part of the analysis presented is directly applicable to the determination of the effects of eccentric transverse prestress in prestressed concrete bridges.

Theoretical Analysis

The complete analysis of the effects of edge-stiffening beams is given elsewhere [5]. Only the basic equations for the various effects are given here, for it is these that are of interest to the designer.

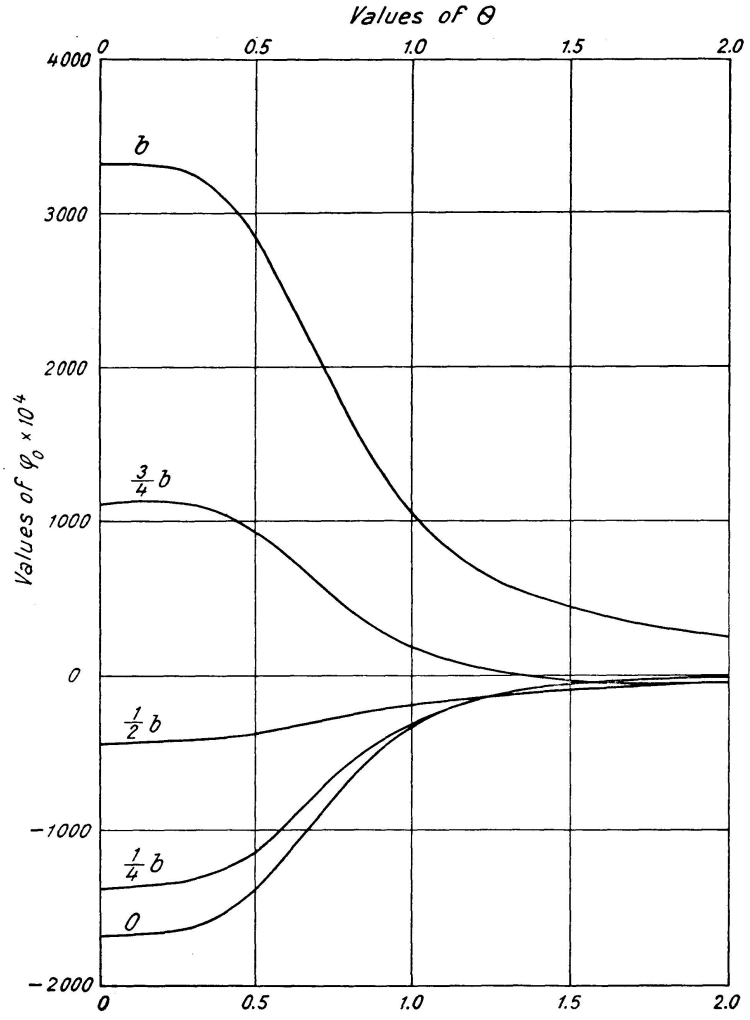

Fig. 1. Values of coefficient φ_0 at points across width of a no-torsion grillage for the deflexions caused by symmetrical edge moments.

a) Symmetrical Edge Moments

The deflexion of the bridge at any point is given by

$$w_1 = -\frac{M_0 b^2}{\rho_E} \sin \frac{\pi x}{2a} \varphi, \tag{1}$$

where φ is a coefficient dependent on θ (the flexural parameter), α (the torsional parameter), and the point in the width of the bridge where the deflexion is required; $M_0 \sin \frac{\pi x}{2a}$ is the applied edge moment.

The slope at the edge of the bridge is given by

$$\left(\frac{\partial w_1}{\partial y}\right)_{y=b} = -\frac{M_0 b}{\rho_E} \sin \frac{\pi x}{2a} \gamma, \tag{2}$$

where γ is a coefficient dependent on θ and α.

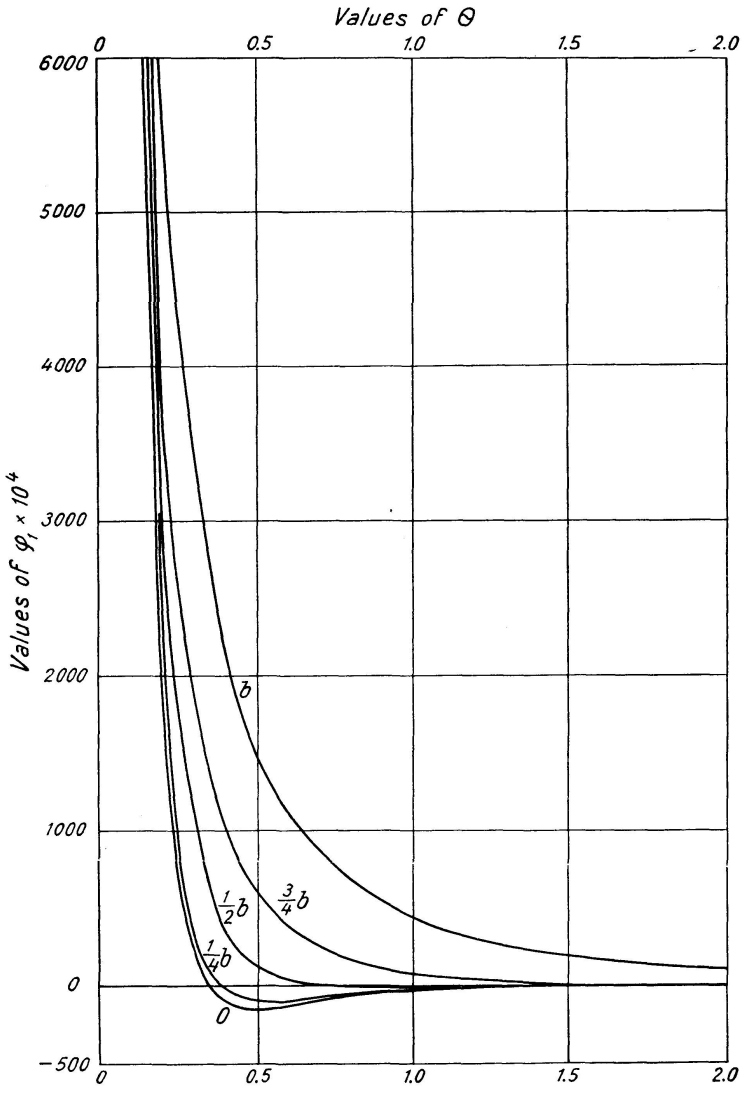

Fig. 2. Values of coefficient φ_1 at points across width of a slab for the deflexions caused by symmetrical edge moments.

The transverse bending moment M_{y_1} is given by

$$M_{y_1} = M_0 \sin\frac{\pi x}{2a}\psi, \tag{3}$$

where ψ is a coefficient dependent on θ, α, and the point in the width of the bridge at which the moment is required.

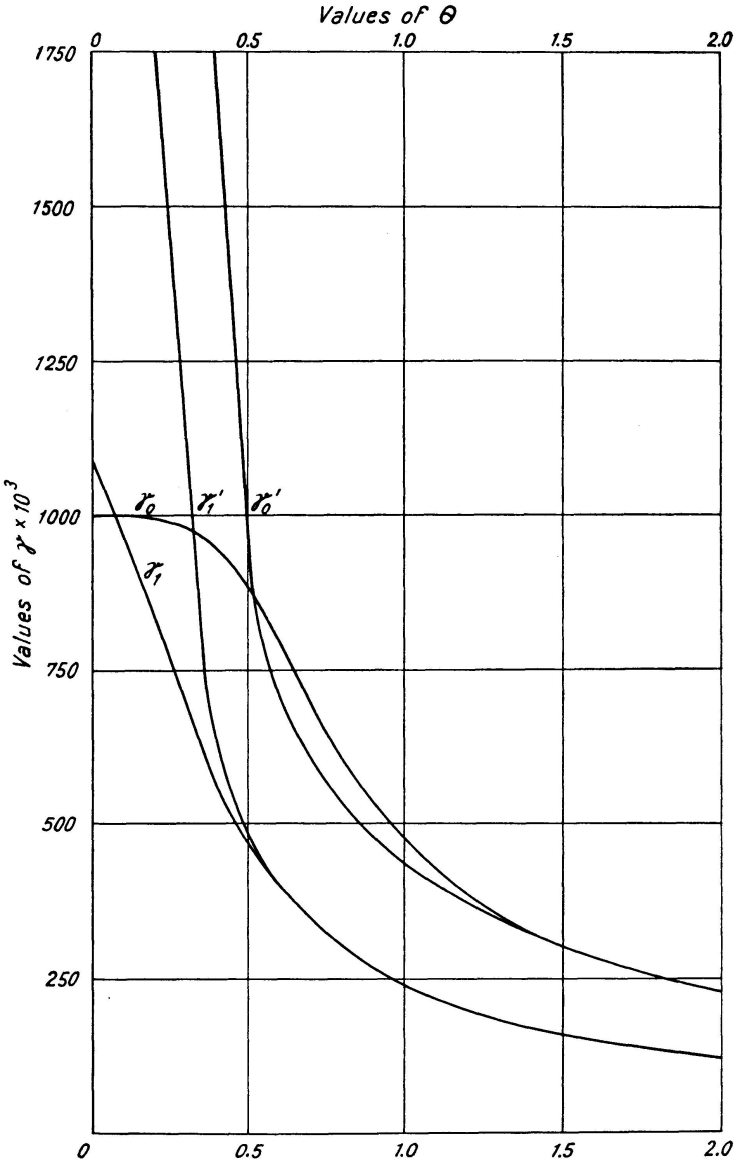

Fig. 3. Values of coefficient giving the slope at $y = +b$ for a no-torsion grillage and a slab for symmetrical and asymmetrical edge moments. For values of γ_0' for θ between 0.1 and 0.4 use linear interpolation between values tabulated below:

θ	0.1	0.2	0.4
γ_0'	315.994	19.734	1.686

Actual values of γ_0'.

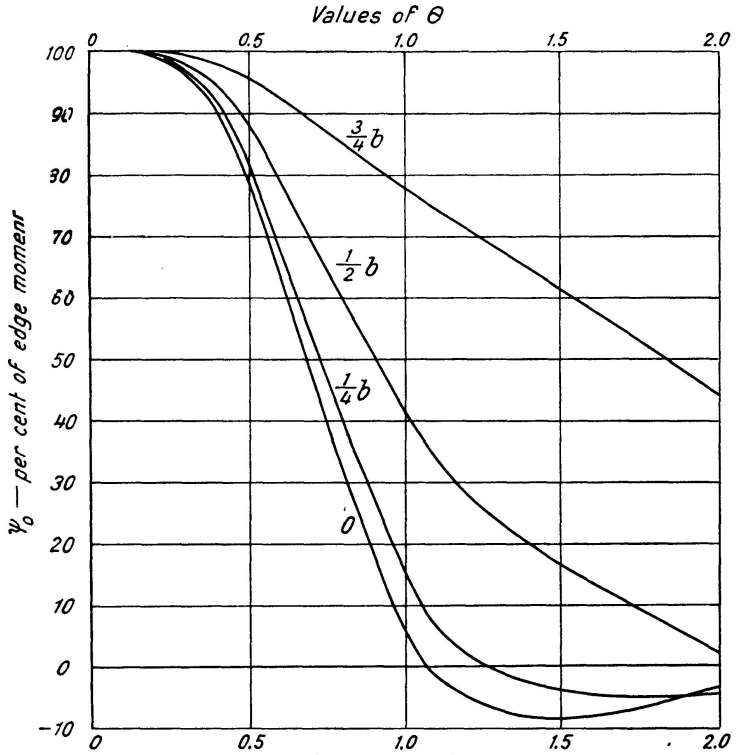

Fig. 4. Values of coefficient ψ_0 for the transverse moment at points across the width of a no-torsion grillage, expressed as a percentage of the edge moment, for symmetrical edge moments.

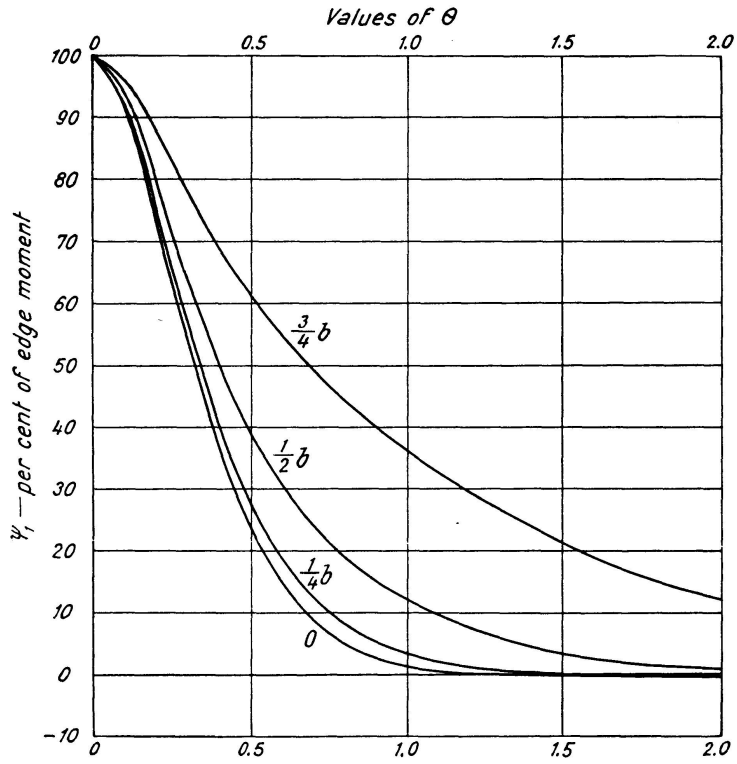

Fig. 5. Values of coefficient ψ_1 for the transverse moment at points across the width of a slab, expressed as a percentage of the edge moment, for symmetrical edge moments.

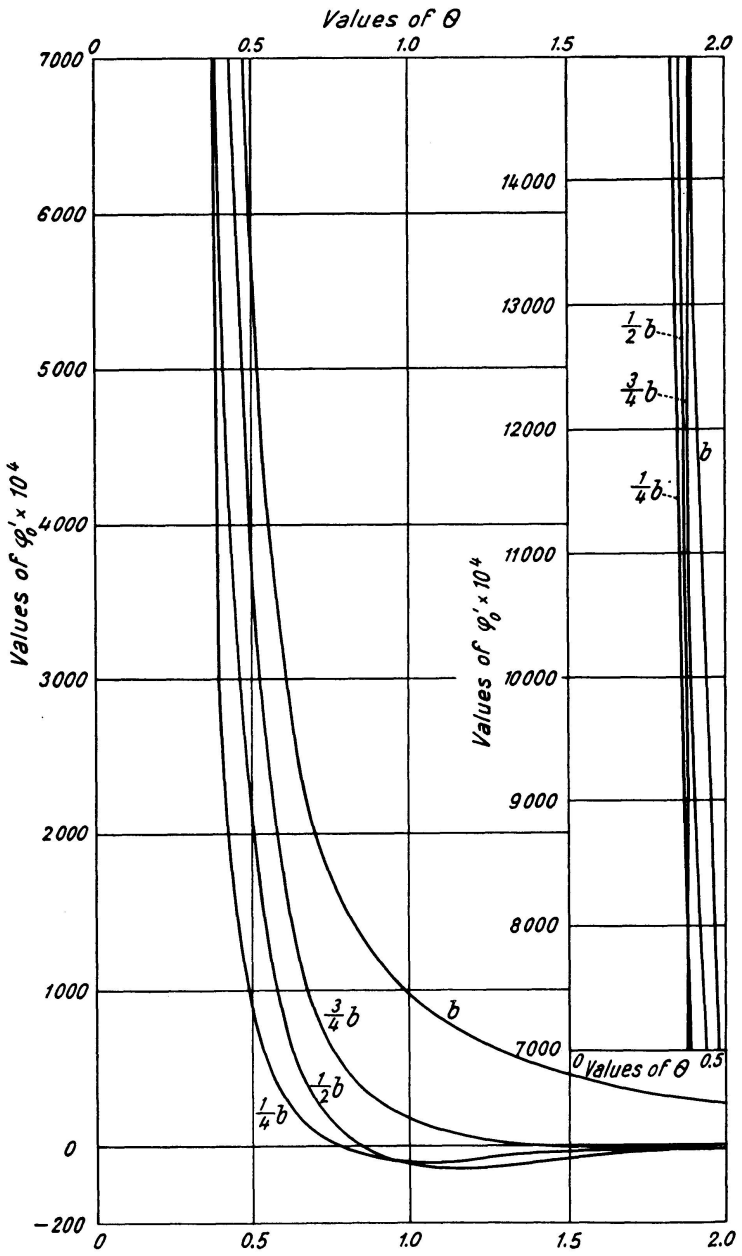

Fig. 6. Values of coefficient φ_0' at points across width of a no-torsion grillage for the deflexions caused by asymmetrical edge moments. For values of θ between 0.1 and 0.4 use linear interpolation between values tabulated below:

θ	0.1	0.2	0.4
0	0	0	0
$b/4$	77.1546	4.7812	0.2702
$b/2$	154.3308	9.5859	0.5628
$3b/4$	231.5507	14.4313	0.8974
b	308.8519	19.3342	1.2880

Actual values of φ_0'.

b) Asymmetrical Edge Moments

This case is similar to (a) and the deflexion, slope, and transverse moment can be expressed in an identical manner i. e.

$$w_1 = -\frac{M_0 b^2}{\rho_E} \sin\frac{\pi x}{2a} \varphi', \tag{4}$$

$$\left(\frac{\partial w_1}{\partial y}\right)_{y=b} = -\frac{M_0 b}{\rho_E} \sin\frac{\pi x}{2a} \gamma', \tag{5}$$

$$M_{y_1} = M_0 \sin\frac{\pi x}{2a} \psi'. \tag{6}$$

The coefficients φ, γ, ψ, φ', γ', and ψ' have been calculated for values of the torsional parameter α of zero and unity. The notation used to denote the coefficients for these extreme cases is

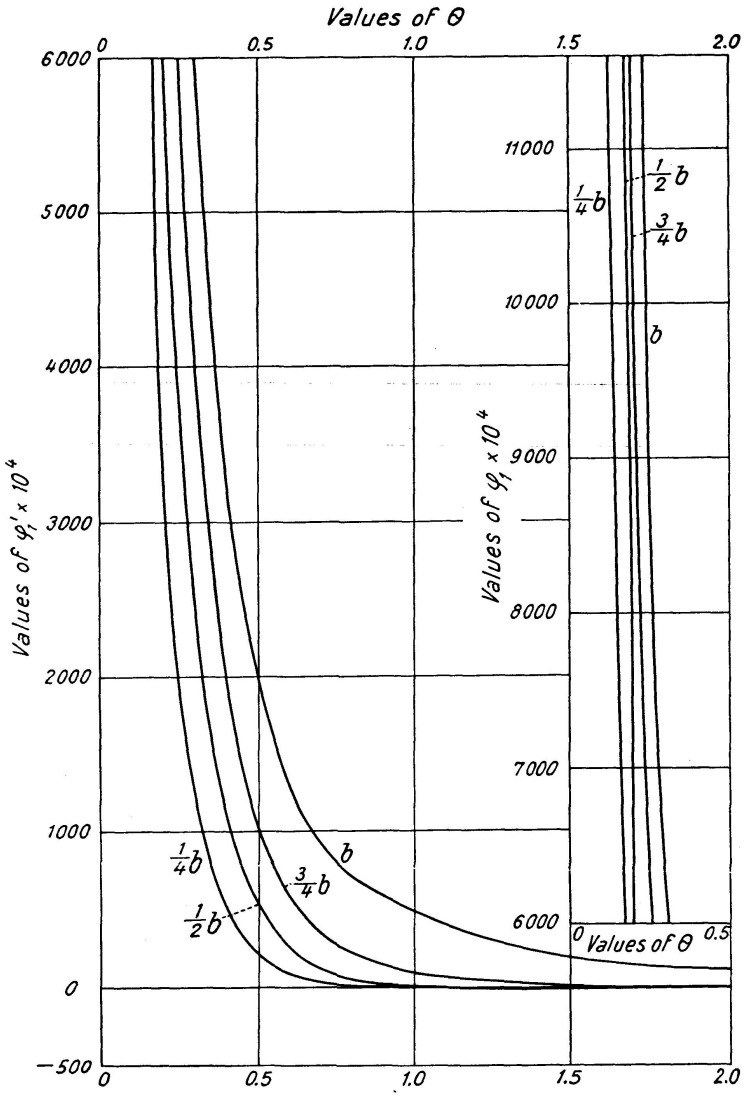

Fig. 7. Values of coefficient φ_1' at points across width of a slab for the deflexions caused by asymmetrical edge moments.

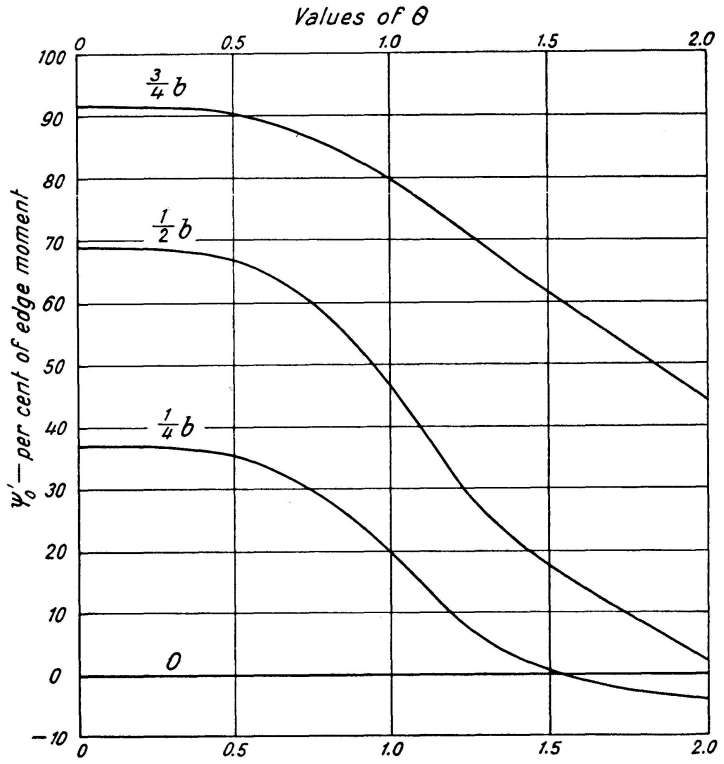

Fig. 8. Values of coefficient ψ_0' for the transverse moment at points across the width of a no-torsion grillage, expressed as a percentage of the edge moment, for asymmetrical edge moments.

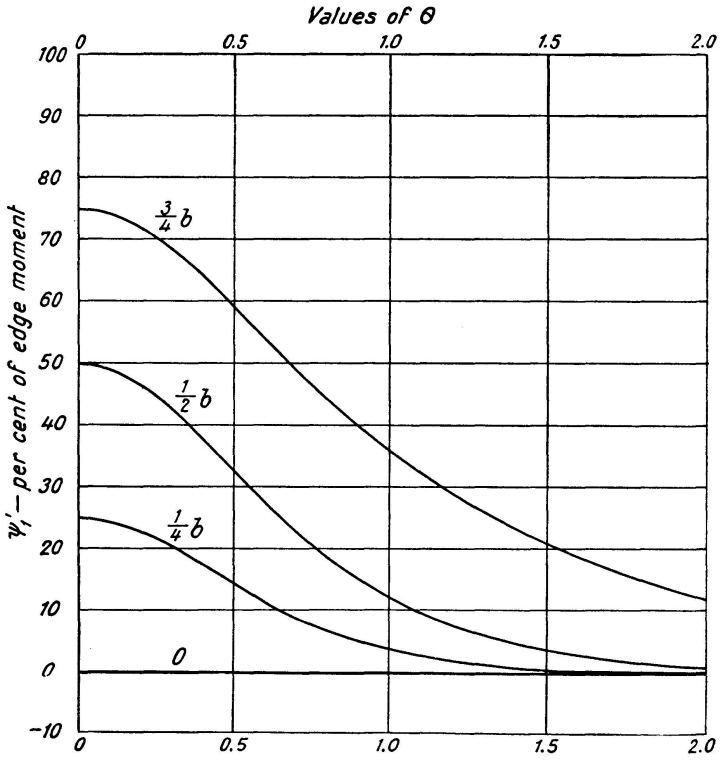

Fig. 9. Values of coefficient ψ_1' for the transverse moment at points across the width of a slab, expressed as a percentage of the edge moment, for asymmetrical edge moments.

$$\varphi_0 = \text{value of } \varphi \text{ when } \alpha = 0,$$
$$\varphi_1 = \text{value of } \varphi \text{ when } \alpha = 1$$

and similarly for the other coefficients.

These coefficients are presented graphically in figs. 1 to 9 for φ_0, φ_1, γ, ψ_0, ψ_1, φ_0', φ_1', ψ_0', and ψ_1' respectively. For intermediate values of α an interpolation formula has been verified which is of the same form for each of the above coefficients. It is

$$Y_\alpha = Y_0 + (Y_1 - Y_0)\sqrt{\alpha}, \tag{7}$$

where Y is representative of φ, γ, or ψ.

c) Deflexion at the Edge of an Anisotropic Bridge Caused by Loads Applied Perpendicularly to the Bridge Surface

The deflexion at the edge of an anisotropic bridge due to applied loading can be determined from the normal load distribution analysis [1]. The deflexion is given by

$$w_1 = \left\{\frac{16\,a^4}{\pi^4 \rho_P}\,\frac{H_1}{2b}\sin\frac{\pi x}{2a}\right\}(K_b \text{ or } K_{-b}). \tag{8}$$

K_b and K_{-b} are dependent on θ, α, and the disposition of the loads across the transverse width of bridge. The normal interpolation used in the distribution analysis applies, i.e.

$$K_\alpha = K_0 + (K_1 - K_0)\sqrt{\alpha}.$$

d) Slope at the Edge of an Anisotropic Bridge Caused by Loads Applied Perpendicularly to the Bridge Surface

The slope is given by

$$\left(\frac{\partial w_1}{\partial y}\right)_{y=b} = \frac{H_1 a^2}{\rho_E}\sin\frac{\pi x}{2a}K', \tag{9}$$

where K' is a coefficient dependent on θ, α, and the disposition of the applied loads across the transverse width of the bridge.

The coefficient K' has been calculated for various values of θ and for a number of values of α; figs. 10 and 11 give the values of K' for $\alpha = 0$ and $\alpha = 1$ respectively. For intermediate values of α the interpolation formula used is

$$K'_\alpha = K'_0 + (K'_1 - K'_0)\sqrt{\alpha}. \tag{10}$$

It should be noted that the calculation of the various coefficients for slab bridges, i.e. $\alpha = 1$, includes the effect of a Poisson's ratio of 0.15 which is applicable to reinforced and prestressed concrete. This was necessary as the effect of Poisson's ratio may be considerable [6].

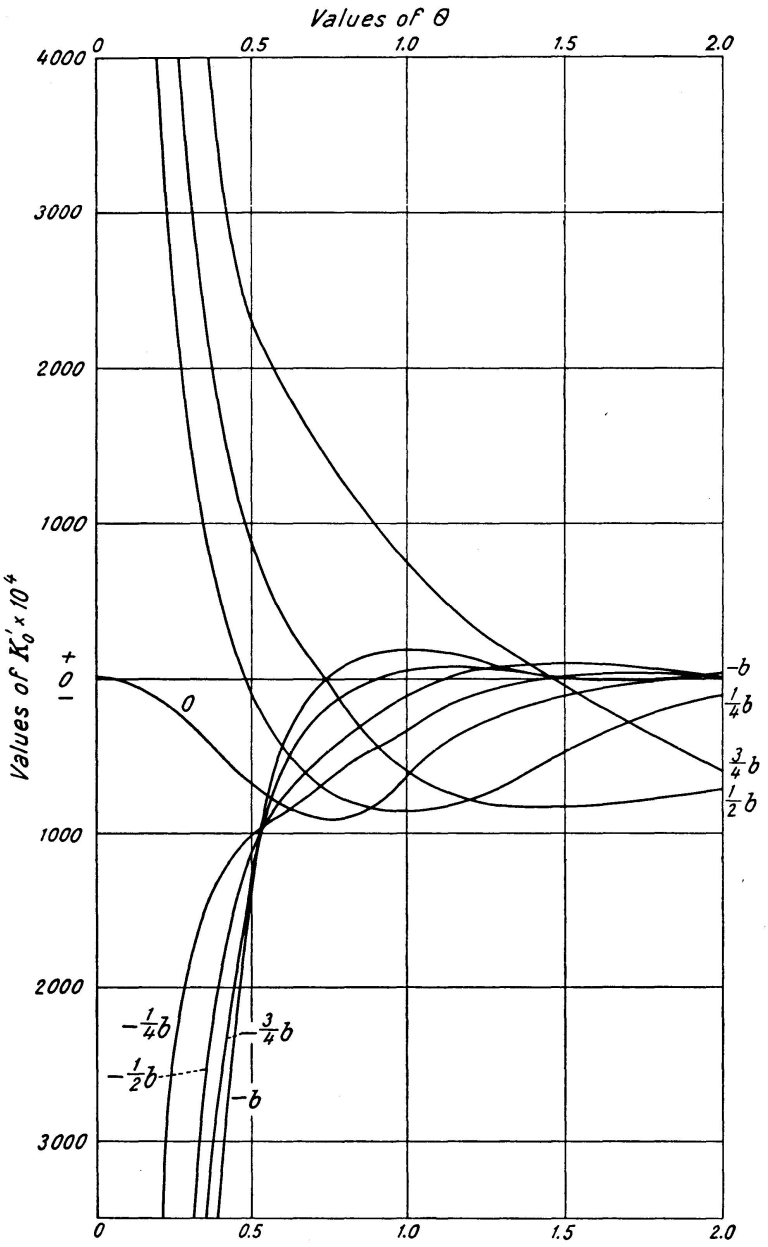

Fig. 10. Values of coefficient K_0' giving the slope at $y = +b$ due to loads applied at points across the width of a no-tension grillage.

Values of K_0' outside scope of curves

θ	0.2	0.25	0.3	0.4	0.5	0.6	1.0	1.495	2.0
b	1.5716	1.1488	0.8260	0.5075	0.4297	0.4159	0.4057	0.4060	0.4054
$\frac{3}{4}b$	1.1623	0.8622	0.5620	—	—	—	—	—	—
$\frac{1}{2}b$	0.7627	0.4380	—	—	—	—	—	—	—
$-\frac{1}{2}b$	−0.07693	−0.5200	−0.3680	—	—	—	—	—	—
$-\frac{3}{4}b$	−1.1441	−0.6500	−0.5000	—	—	—	—	—	—
$-b$	−1.5185	−1.1142	−0.7100	—	—	—	—	—	—

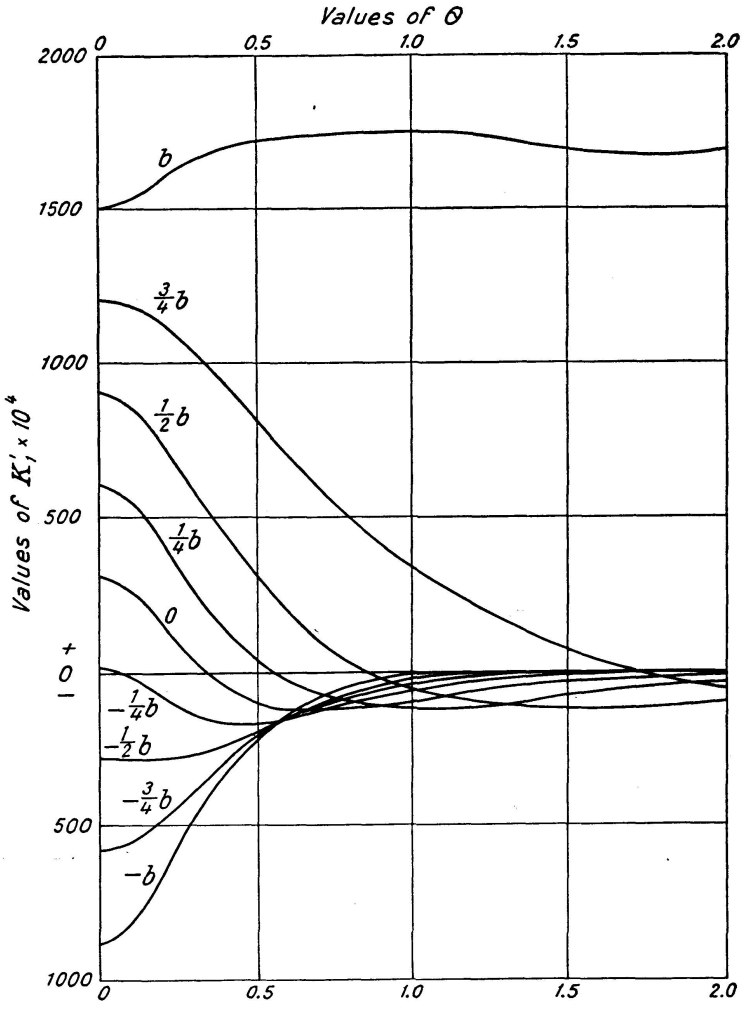

Fig. 11. Values of coefficient K_1' giving the slope at $y = +b$ due to loads applied at points in the width of a slab.

e) General Solution for the Effect of Edge-Stiffening Beams on an Anisotropic Bridge

Consider the bridge with edge-stiffening beams in fig. 12a. Let the span of the bridge be $2a$, the width of the uniform section of the bridge (i. e. excluding width of edge beams) be $2b$, the stiffness per unit length of the longitudinal section be ρ_E, the moment of inertia of the edge beams be I_E, and the torsional stiffness of the edge beams be J_E. The applied loading is represented by the four equal loads D.

The edge beams can be isolated from the remainder of the bridge and edge shear forces and moments introduced as shown in fig. 12b. These shear forces and edge moments are assumed to be distributed sinusoidally along the span.

The bridge can now be analysed using the results obtained in sections (a), (b), (c), and (d), and the unknown shear forces F_1 and F_2 and edge moments

M_1 and M_2 determined from the compatibility equations for deflexion and slope at the edge $y = \pm b$.

The shear forces F_1 and F_2 can be treated as applied loads on the bridge and hence the deflexion at the edge $y = b$ due to all the applied loads can be written:

$$\delta_{y=b} = \frac{16a^4}{\pi^4 \rho_P} \frac{H_1}{2b} \sin\frac{\pi x}{2a} (K_b \text{ due to } P) - \frac{16a^4}{\pi^4 \rho_P} \sin\frac{\pi x}{2a} \left(\frac{F_1}{2b} K_b + \frac{F_2}{2b} K_{-b} \right), \quad (11)$$

where H_1 is the amplitude of the first term in the Fourier series for the applied loads P.

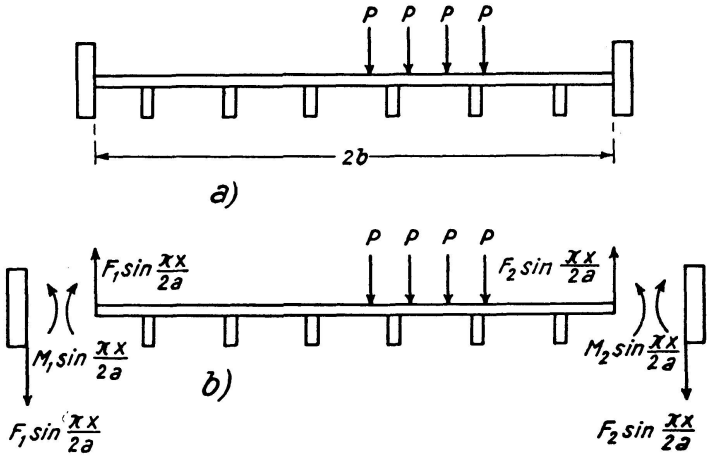

Fig. 12.
(a) Bridge considered in analysis.
(b) Forces and moments acting on bridge and edge beams.

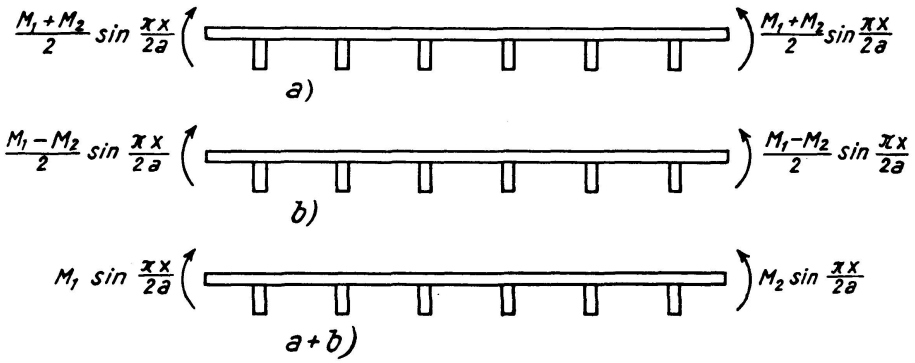

Fig. 13. Superposition of symmetrical and asymmetrical edge moments to obtain desired edge moments.

The edge moments M_1 and M_2 can be considered in the form shown in fig. 13. This method of superposing symmetrical and asymmetrical edge moments enables the coefficients φ to be used. Thus the deflexion at the edge $y = b$ due to the edge moments can be written:

$$\delta_{y=b} = -\left\{ \frac{M_1 + M_2}{2} \frac{b^2}{\rho_E} \varphi_b + \frac{M_1 - M_2}{2} \frac{b^2}{\rho_E} \varphi_b' \right\} \sin\frac{\pi x}{2a}. \quad (12)$$

The total deflexion given by the sum of eqs. (11) and (12) must equal that of the edge beam at $y=b$ under the action of the loading $F_1 \sin\frac{\pi x}{2a}$. Therefore for compatibility of deflexion the following equation must be satisfied.

$$\begin{aligned}\frac{16a^4}{\pi^4 E I_E} F_1 \sin\frac{\pi x}{2a} = {} & \frac{16a^4}{\pi^4 \rho_P} \sin\frac{\pi x}{2a}\left\{\frac{H_1}{2b}(K_b \text{ due to } P) - \frac{F_1}{2b}K_b - \frac{F_2}{2b}K_{-b}\right\} \\ & - \frac{b^2}{2\rho_E}\sin\frac{\pi x}{2a}\{(M_1+M_2)\varphi_b + (M_1-M_2)\varphi_b'\}.\end{aligned} \tag{13}$$

Similarly at $y=-b$:

$$\begin{aligned}\frac{16a^4}{\pi^4 E I_E} F_2 \sin\frac{\pi x}{2a} = {} & \frac{16a^4}{\pi^4 \rho_P} \sin\frac{\pi x}{2a}\left\{\frac{H_1}{2b}(K_{-b} \text{ due to } P) - \frac{F_1}{2b}K_{-b} - \frac{F_2}{2b}K_b\right\} \\ & - \frac{b^2}{2\rho_E}\sin\frac{\pi x}{2a}\{(M_1+M_2)\varphi_b - (M_1-M_2)\varphi_b'\}.\end{aligned} \tag{14}$$

For slope compatibility at the edge $y=b$, it is found that for the bridge:

$$\begin{aligned}\left(\frac{\partial w_1}{\partial y}\right)_{y=b} = {} & \frac{a^2}{\rho_E}\sin\frac{\pi x}{2a}\{H_1(K_b' \text{ due to } P) - F_1 K_b' - F_2 K_{-b}'\} \\ & - \frac{b}{\rho_E}\sin\frac{\pi x}{2a}\left\{\left(\frac{M_1+M_2}{2}\right)\gamma_b + \left(\frac{M_1-M_2}{2}\right)\gamma_b'\right\}.\end{aligned} \tag{15}$$

For the torsion of the edge beam subjected to a twisting moment varying sinusoidally over the span, the angle of twist at any point may be determined by integrating between the desired limits the product of the moment at any point and the distance of the point from the origin. Thus the edge beam rotation at a distance x from the abutment is

$$\frac{\int_0^x M_1 x \sin\frac{\pi x}{2a} dx}{G J_E}. \tag{16}$$

The compatibility equation for slope at $y=b$ is therefore

$$\begin{aligned}\frac{\int_0^x M_1 x \sin\frac{\pi x}{2a} dx}{G J_E} = {} & \frac{a^2}{\rho_E}\sin\frac{\pi x}{2a}\{H_1(K_b' \text{ due to } P) - F_1 K_b' - F_2 K_{-b}'\} \\ & - \frac{b}{\rho_E}\sin\frac{\pi x}{2a}\left\{\left(\frac{M_1+M_2}{2}\right)\gamma_b + \left(\frac{M_1-M_2}{2}\right)\gamma_b'\right\},\end{aligned} \tag{17}$$

and similarly at $y=-b$

$$\begin{aligned}\frac{\int_0^x M_2 x \sin\frac{\pi x}{2a} dx}{G J_E} = {} & \frac{a^2}{\rho_E}\sin\frac{\pi x}{2a}\{H_1(K_{-b}' \text{ due to } P) - F_1 K_{-b}' - F_2 K_b'\} \\ & - \frac{b}{\rho_E}\sin\frac{\pi x}{2a}\left\{\left(\frac{M_1+M_2}{2}\right)\gamma_b - \left(\frac{M_1-M_2}{2}\right)\gamma_b'\right\}.\end{aligned} \tag{18}$$

Eqs. (13), (14), (17), and (18) enable the unknown edge effects F_1, F_2, M_1, and M_2 to be determined. For this purpose it is sufficient to consider the mid-span section of the bridge, i.e. $x=a$. Once these values have been determined the deflections, the longitudinal and transverse moments at any point in the bridge, and the bending and torsional moments at any point in the egde beams may be determined by superposing the various effects.

It will be noted that all the curves given are for the edge $y=b$. The appropriate values for the edge $y=-b$ can be obtained either from these curves by using the Reciprocal Theorem and taking note of the sign convention used, or by treating each edge as $y=b$ in turn, adjusting the load positions and using the actual values obtained from the curves.

Application of the Theoretical Analysis to Two Types of Model Bridge

To check the validity of the theory, tests were made on two model bridges subjected to a number of concentrated loads; one of the models was a slab bridge and one a beam and slab bridge.

a) Slab Bridge with Edge-Stiffening Beams

The Perspex model is shown in fig. 14. The span $2a$ was 18.90 in., the width $2b$ was 22.68 in., the slab thickness h was 0.70 in., and the edge beams had the dimensions 1.26×0.42 in.

The distribution of deflexion due to a scale model of the M. O. T. abnormal vehicle with its transverse wheel positions as shown in fig. 15 was measured with and without edge beams and compared with the theoretical results derived from the analysis given previously.

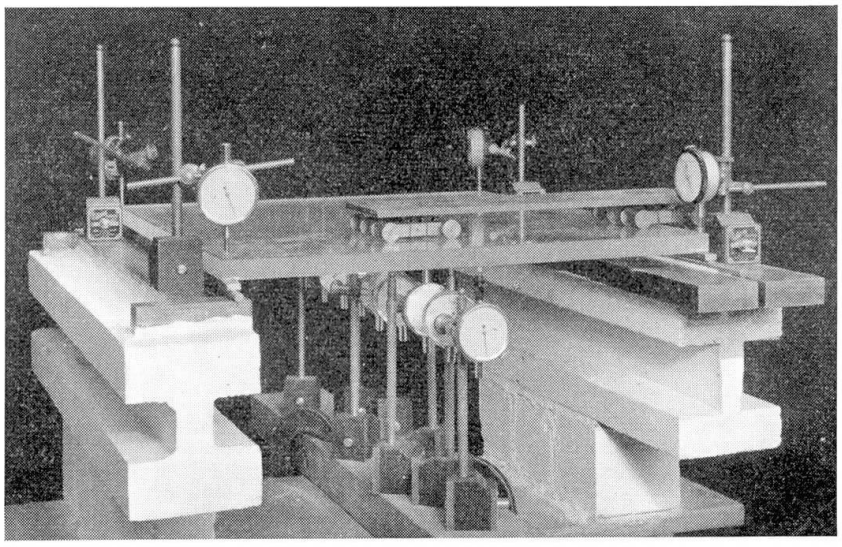

Fig. 14a. Slab bridge without edge beams.

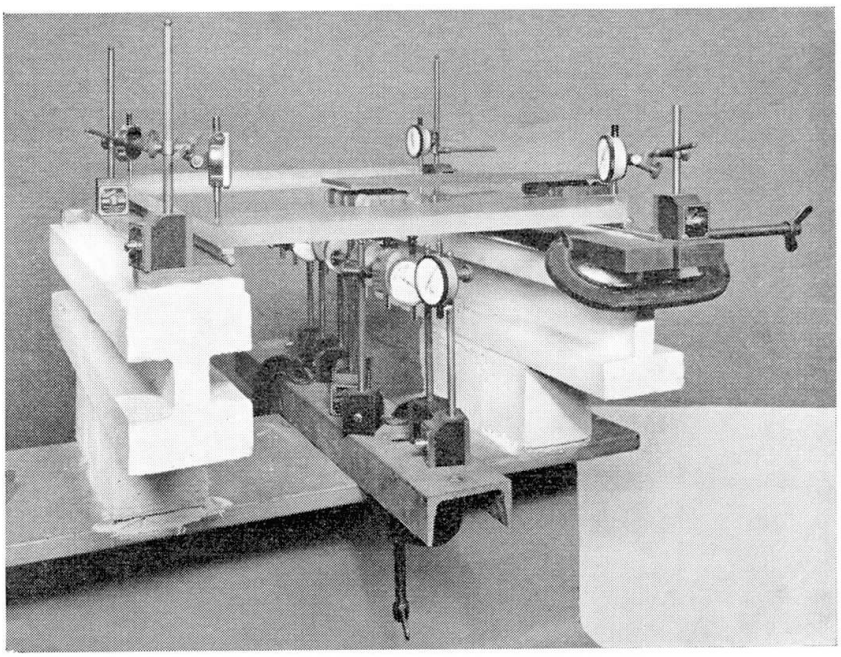

Fig. 14b. Slab bridge with edge beams.

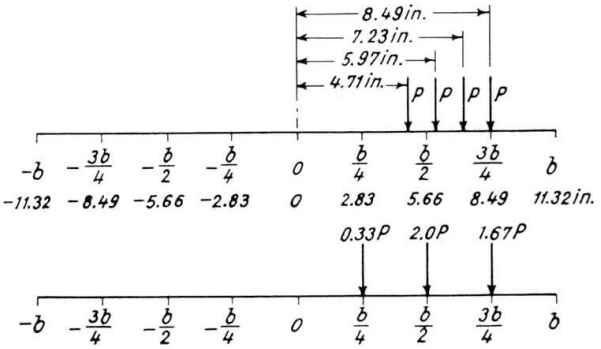

Fig. 15. Transverse position of load on slab bridge and distribution to standard positions.

Fig. 16. Forces acting on slab bridge at mid-span.

The forces and moments acting on the bridge are shown in fig. 16, and the longitudinal positions of the axles of the abnormal load are as shown in fig. 17.

The appropriate coefficients obtained from figs. 1 to 9 for a value of θ of 0.6 and all the relevant data needed for the derivation of the compatibility equations are given in table 1. The values of the normal distribution coefficient K and the slope coefficient K' were obtained by replacing the wheel loads by equivalent loads at the standard positions, as shown in fig. 15, and weighting the coefficients for these positions accordingly.

The compatibility equations can now be derived; this derivation for the mid-span section of the bridge is shown in table 2. For convenience the value

of $1/E$ has been omitted from the values for the deflexions and slopes since it is a common factor. The four compatibility equations are obtained by equating the deflexions and slopes at the two edges of the slab to the deflexion and rotation at the edge beams.

Solving these equations the values for the shear forces and edge moments are found to be

$$F_1 = 0.117\,P; \qquad F_2 = 0.028,$$
$$M_1 = 0.100\,P; \qquad M_2 = -0.048.$$

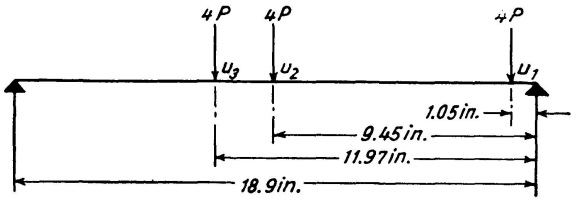

Fig. 17. Longitudinal position of loads on slab bridge.

Table 1. Slab Bridge — Fundamental Data Required for Derivation of Compatibility Equations

$2a$ = 18.90 in. $D = \dfrac{E h^3}{12(1-\nu^2)} = 0.0292\,E$ when $\nu = 0.15$

$2b$ = 22.68 in. Edge beam: width = 0.42 in., depth = 1.26 in.

h = 0.70 in. Torsional stiffness of edge beam = $0.0107\,E$

Flexural parameter $\theta = \dfrac{b}{2a} = 0.6$

Coefficient	Value at	
	Edge $y = +b$	Edge $y = -b$
K (due to loads P)	1.642	0.406
K (due to shears F)	2.531	0.263
φ symmetrical moments	0.111	0.111
φ' asymmetrical moments	0.13	0.13
K' (due to loads P)	0.1548	0.0598
K' (due to shears F)	0.1735	0.0142
γ symmetrical moments	0.397	0.397
γ' asymmetrical moments	0.396	0.396

P = wheel load of abnormal vehicle.

Amplitude of 1st term of Fourier series for abnormal load, H_1,

$$H_1 = \frac{4P}{b}\left\{\sin\frac{\pi u_1}{2a} + \sin\frac{\pi u_2}{2a} + \sin\frac{\pi u_3}{2a}\right\}$$

for axle positions as in fig. 17 = $0.8835\,P$. "Mean" deflexion under abnormal loading, W_1,

$$W_1 = \frac{16a^4}{\pi^4 D}\frac{H_1}{2b}\sin\frac{\pi x}{2a} = 174.03\frac{P}{E}\sin\frac{\pi x}{2a}$$

Table 2. Slab Bridge — Derivation of Compatibility Equations

Operative forces or moments	Deflexions		Slopes	
On slab	Edge $+b$	Edge $-b$	Edge $+b$	Edge $-b$
Loads P	$2{,}865.34\ P$	$713.72\ P$	$417.67\ P$	$161.35\ P$
Shear force F_1	$-4{,}999.65\ F_1$	$-518.89\ F_1$	$-529.57\ F_1$	$-43.37\ F_1$
Shear force F_2	$-518.89\ F_2$	$-4{,}999.65\ F_2$	$43.37\ F_2$	$529.57\ F_2$
Symmetrical moments $\left(\frac{M_1+M_2}{2}\right)$	$-488.15\left(\frac{M_1+M_2}{2}\right)$	$-488.15\left(\frac{M_1+M_2}{2}\right)$	$-153.96\left(\frac{M_1+M_2}{2}\right)$	$153.96\left(\frac{M_1+M_2}{2}\right)$
Asymmetrical moments $\left(\frac{M_1-M_2}{2}\right)$	$-571.71\left(\frac{M_1-M_2}{2}\right)$	$571.71\left(\frac{M_1-M_2}{2}\right)$	$-153.57\left(\frac{M_1-M_2}{2}\right)$	$-153.57\left(\frac{M_1-M_2}{2}\right)$
On edge beam				
Shear forces F_1 and F_2	$18{,}709.81\ F_1$	$18{,}709.81\ F_2$		
Twisting moments M_1 and M_2			$3{,}388.85\ M_1$	$-3{,}388.85\ M_2$

Sign convention: Downward deflexion positive.

Slope is positive if it results in a clockwise rotation of edge beam, i.e. as shown in fig. 16, F_1 causes negative edge slopes and F_2 causes positive edge slopes; the symmetrical moments cause a negative slope at b and a positive slope at $-b$ and the asymmetrical moments cause negative slopes at both edges.

The above values were checked using six decimal places in the initial equations; the results obtained from this procedure were:

$$F_1 = 0.117890; \qquad F_2 = 0.028782,$$
$$M_1 = 0.100539; \qquad M_2 = -0.048413,$$

where the shear forces were determined first.

The agreement between the two sets of values is good; this is so only when great care is taken in deriving values from equations in which only two decimal points are considered. It is essential that F_1 and F_2 be obtained first and that subsequent substitutions for M_1 and M_2 are carried out in equations where the coefficients are all small, i. e. approximately unity or less.

The forces acting on the slab are, therefore, as shown in fig. 18 where the edge moments have been separated into their symmetrical and asymmetrical components.

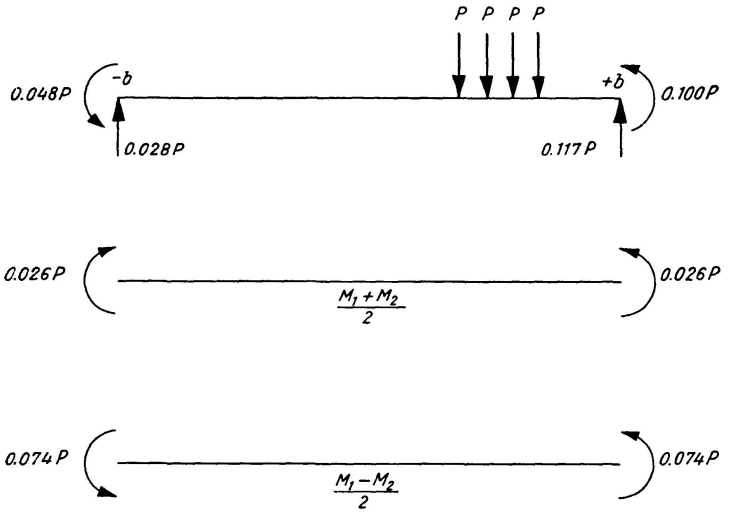

Fig. 18. Forces acting at mid-span of slab bridge with edge-stiffening beams.

The above solution is exact in that all the possible forces have been considered. It is interesting, however, to solve the problem without including the effects of edge moments. The solution is simplified considerably as there are then only two unknowns F_1 and F_2. Only deflexion compatibility need be considered and from table 2 the following compatibility equations are obtained by omitting the terms in M:

$$0 = 2865.34\,P - 23{,}709.46\,F_1 - 518.89\,F_2,$$
$$0 = 713.72\,P - 518.89\,F_2 - 23{,}709.46\,F_1,$$

whence

$$F_1 = 0.120\,P; \qquad F_2 = 0.028\,P.$$

Here again it is necessary to exercise care in determining F_1 and F_2 if only two decimal places are considered, as the equations are ill-conditioned.

From the deduced values of the shearing forces, F, and the edge moments, M, the theoretical deflexion profiles can be obtained.

Table 3 compares the theoretical and experimental deflexions for a value of P of 1.798 lb. and a measured E of 4.825×10^{-5} lb./in^2. From the table it will be seen that (a) the effect of the edge moments, M, on the theoretical values is very small and can well be neglected and (b) the agreement between the theoretical and experimental values is good especially in the region of the applied load. The theoretical and experimental "mean" deflexions checked well in each case and were 63.62×10^{-4} in. and 62.74×10^{-4} in. for the unstiffened bridge and 52.3×10^{-4} in. and 53.64×10^{-4} in. for the stiffened bridge. This confirms that the "mean" effects are proportional to the over-all longitudinal stiffness of a bridge.

Table 3. Theoretical and Experimental Deflexion Profiles at the Mid-Span Section of Slab Bridge With and Without Edge-Stiffening Beams

Position on section	Deflexions in 0.0001 in. due to				
	P	Experimental	$P+F$	$P+F+M$	Experimental
$-b$	26.62	28.1	19.09	20.18	14.4
$-3b/4$	32.34	30.2	25.34	25.89	20.2
$-b/2$	39.83	37.6	32.96	33.26	27.7
$-b/4$	49.65	44.1	42.30	43.50	36.8
0	62.67	57.2	54.07	53.85	47.1
$b/4$	77.57	73.7	66.82	66.90	63.8
$b/2$	91.63	88.8	77.73	77.61	75.8
$3b/4$	101.06	100.5	83.00	82.39	81.4
b	106.85	116.5	83.90	82.21	86.3

Because the measured maximum deflexions were greater than the theoretical values it was decided to investigate the solution further by including the effects of Poisson's ratio, ν, in the distribution coefficients K [6]. It has been found that in the case of concrete for which ν has a mean value of 0.15 these effects are negligible. However, this is not necessarily so for higher values of ν, and since $\nu = 0.25$ for the Perspex used the point was worth investigating.

The distribution coefficients K were re-calculated for $\theta = 0.6$ and for $\nu = 0.25$; with these values a new set of compatibility equations was derived assuming that the edge moments could be ignored. The solution to these equations yielded

$$F_1 = 0.131\ P \quad \text{and} \quad F_2 = 0.029\ P.$$

From these values table 4 was produced; it compares theoretical and experimental deflexions for a value of P of 1.748 lb. and a measured E of 4.825×10^5 lb./in^2 i. e. it is for the same loading as table 3. A study of tables 3

and 4 shows that the maximum experimental deflexions lie between the theoretical values derived by assuming Poisson's ratio is zero or 0.25. It may thus be concluded that for concrete it will be sufficient to assume $\nu = 0$ in calculation since even for Perspex the error in this assumption was only 5% and would be less for concrete.

Table 4. Theoretical and Experimental Deflexion Profiles at the Mid-Span Section of Slab Bridge With and Without Edge-Stiffening Beams when Poisson's Ratio $\nu = 0.25$

Position on section	Deflexions in 0.0001 in. due to			
	P	Experimental	$P+F$	Experimental
$-b$	27.07	28.1	17.72	14.4
$-3b/4$	31.24	30.2	23.05	20.2
$-b/2$	38.26	37.6	30.44	27.7
$-b/4$	48.48	44.1	40.13	36.8
0	62.08	57.2	52.18	47.1
$b/4$	78.29	73.7	65.62	63.8
$b/2$	94.62	88.8	77.73	75.8
$3b/4$	108.45	100.5	85.69	81.4
b	121.95	116.5	91.49	86.3

The longitudinal bending moments are found by replacing the factor $\frac{16a^4}{\pi^4 D 2b}$ in the expression for the "mean" deflexion due to live load and edge shearing forces by the factor $\frac{4a^2}{\pi^2 2b}$. Thus the mid-span longitudinal moments would be found by multiplying the results of table 3 by $\frac{\pi^2 D}{4a^2}$. Naturally, for an actual bridge, once the values of F_1 and F_2 had been found in terms of P the moments would be found directly as $\frac{4^2 a}{\pi^2 2b}$ $(K_{1_P} H_1 - K_{1_{F_1}} F_1 - K_{1_{F_2}} F_2)$ where K_{1_P}, $K_{1_{F_2}}$ and $K_{1_{F_1}}$ are the relevant coefficients K_1 for each force at the point on the transverse section under consideration.

Transverse bending moments. The transverse bending moments will also be modified by the forces induced along the edges of the bridge. The maximum possible transverse moment on any transverse section occurs at the centre of the section. The transverse position of the load to cause this moment is shown in fig. 19. This position does not coincide with the position which has been considered for the determination of the maximum longitudinal effects and therefore the values of F_1 and F_2 will differ from those obtained before. However, a completely new set of compatibility equations is not necessary for the determination of the new values of F_1 and F_2 since the only coefficients to change are those involving P, the terms involving F and M being exactly as before.

The loads can be distributed to the standard positions and the corresponding distribution coefficient profile can then be deduced. The four compatibility equations can be derived in exactly the same way as in table 2, the only values that are different from the values in table 2 being those dependent on the position of the abnormal load vehicle.

For this particular loading the shear forces, F, and edge moments, M, are as shown in fig. 20. The distribution of the transverse moments on the central section can now be found. The moments caused by the abnormal vehicle alone are calculated by the μ-coefficient analysis [5]; the moments due to the shear forces F_1 and F_2 are calculated in a similar manner; the moments due to the edge moments M_1 and M_2 are calculated by using the percentage curves of figs. 5 and 9. Hence the total moment is found; table 5 gives the individual transverse moments at points across the width of the central transverse section caused by the various forces and moments and the total moment at each point.

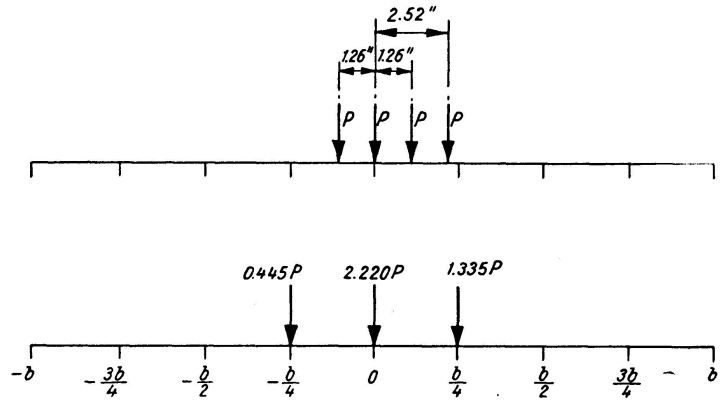

Fig. 19. Distribution of applied loads to standard positions for investigation of the maximum transverse moment in slab bridge.

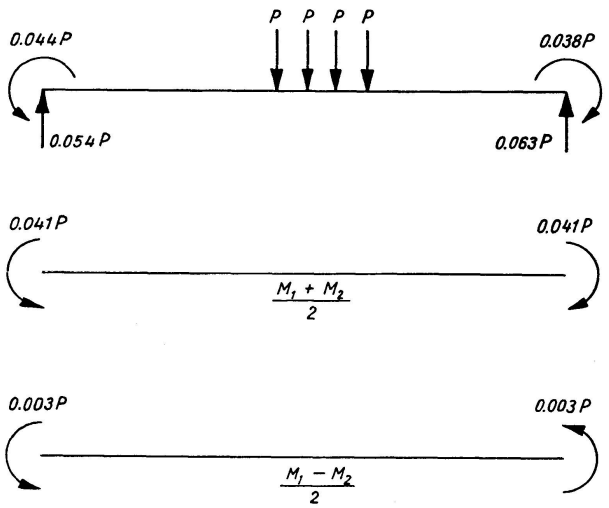

Fig. 20. Forces acting at mid-span of slab bridge with edge-stiffening beams for investigation of maximum transverse moment.

Table 5. Mid-Span Transverse Bending Moments for Slab Bridge With and Without Edge-Stiffening Beams

Position on section	Transverse moment $\left(x \frac{1}{P}\right)$ due to					
	P	F	F	$\frac{M_1+M_2}{2}$	$\frac{M_1-M_2}{2}$	Total moment
$-b$	0	0	0	−0.0410	0.0030	−0.0380
$-3b/4$	−0.0702	0.0089	0.0256	−0.0224	0.0016	−0.0565
$-b/2$	0.0780	0.0164	0.0330	−0.0125	0.0008	0.1157
$-b/4$	0.5946	0.0236	0.0306	−0.0075	0.0004	0.6417
0	1.3995	0.0300	0.0256	−0.0060	0	1.4491
$b/4$	1.0443	0.0357	0.0202	−0.0075	−0.0004	11.0923
$b/2$	0.2509	0.0386	0.0141	−0.0125	−0.0008	0.2903
$3b/4$	−0.0150	0.0300	0.0076	−0.0224	−0.0016	−0.0014
b	0	0	0	−0.0410	−0.0030	−0.0440

It is seen that the over-all effect of stiffening the bridge has been to increase the maximum moment by only 4%. It may be concluded from this that the modifying effects of the edge shears and moments can be ignored. Whether they are ignored in all cases must be left to the designer. The moments caused by the forces P and F and the moment M will all increase with increase in θ and, therefore, the percentage increase in moment will not be affected greatly by variations in plan dimensions. The ratio of the flexural stiffness per inch width of the edge beam to the flexural resistance per inch run of the slab was 5.7 and the ratio of the torsional stiffness per inch width of the edge beam to the torsional stiffness of the slab per inch run was about $^1/_2$. These ratios might be some guide in deciding whether it is worth while considering edge shears and moments in the determination of transverse bending moments. If the ratios are less than those given above the modifying effect on the maximum moment should be less than 4%. Further, if the ratios are greater, it will only be necessary to include the effects of edge moments if the ratio of the flexural stiffness to the torsional stiffness of the edge beam is less than, say, 5.

b) Beam and Slab Bridge with Edge-Stiffening Beams

The previous work has considered the effects of edge-stiffening beams on slab bridges. It is necessary to extend the investigation to include bridges for which $\alpha \neq 0$ since it is then necessary to make use of interpolation formulæ of the type $Y_\alpha = Y_0 + (Y_1 - Y_0)\sqrt{\alpha}$. A Perspex model of a beam and slab bridge, shown in fig. 21, was tested to find the modifying effects of stiffening beams at the edges of the structure. The dimensions and properties of the model are given in table 6.

Table 6. Properties of Beam and Slab Bridge Model

Span 2a	17.81 in.
Width 2b	12 in.
Thickness of slab	0.187 in.
Thickness of rib	0.167 in.
Depth of rib	1.313 in.
Thickness of diaphragm	0.167 in.
ρ_P per inch	0.05448
ρ_E per inch	0.02923
Young's modulus E	3.86×10^5 lb./in^2
Modulus of rigidity G	1.55×10^5 lb./in^2
Flexural parameter θ	0.3900
Torsional parameter α	0.0177
Depth of edge beam	1.98 in.
Thickness of edge beam	0.257 in.
Flexural stiffness of edge beam	0.1662 E
Torsional stiffness of edge beam	0.0102 G

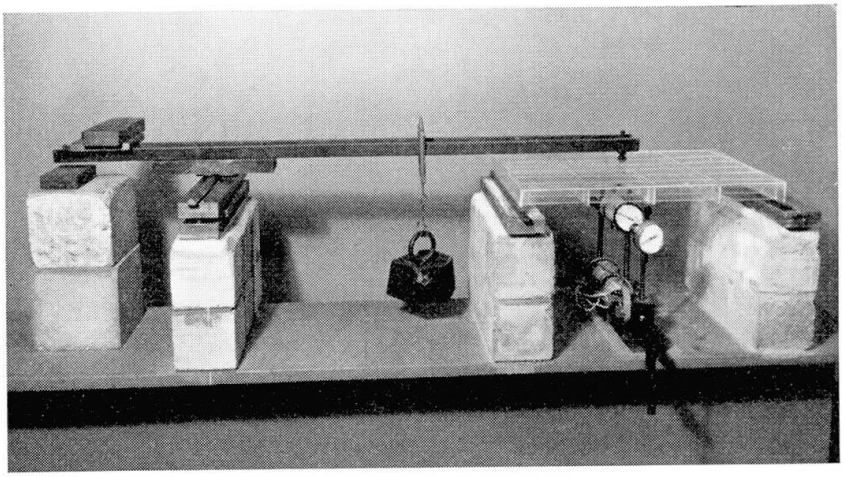

Fig. 21. Perspex beam and slab model under test.

A single load, P, of 5.51 lb. was applied at the point $b/6$ on the mid-span transverse section.

The derivation of the coefficients in the compatibility equations is set out in detail in tables 7 and 8 for deflexion and slope respectively. These tables illustrate the functioning of the interpolation formula mentioned above.

From these coefficients and the equation given in section 2(*c*) the four compatibility equations may be set up. If this is done the solution is found to be

$$F_1 = 0.020\ P, \qquad F_2 = 0.009\ P,$$
$$M_1 = -0.001\ P, \qquad M_2 = -0.002\ P.$$

Table 7. Deflexion Coefficients and "Mean" Factors for Beam and Slab Bridge

Applied load at $+b/6$

Position on section

K_0	$-b$	$-3b/4$	$-b/2$	$-b/4$	0	$b/4$	$b/2$	$3b/4$	b
0.33×0	0.248	0.284	0.323	0.370	0.389	0.370	0.323	0.284	0.248
$0.67 \times b/4$	0.101	0.241	0.422	0.603	0.750	0.844	0.911	0.992	1.052
$\sum K_0$	0.349	0.525	0.745	0.973	1.139	1.214	1.234	1.276	1.300
K_1									
0.33×0	0.302	0.316	0.330	0.345	0.353	0.345	0.330	0.316	0.302
$0.67 \times b/4$	0.528	0.565	0.608	0.654	0.699	0.737	0.739	0.727	0.717
$\sum K_1$	0.830	0.881	0.938	0.999	1.052	1.082	1.069	1.043	1.019
$K_0+(K_1-K_0)\sqrt{\alpha}$	0.413	0.572	0.772	0.977	1.127	1.196	1.212	1.245	1.263

Edge shear force — Load at $+b$

K_0	-1.650	-1.080	-0.540	0.130	0.735	1.570	2.400	3.405	4.250
K_1	0.523	0.596	0.675	0.789	0.917	1.071	1.286	1.532	1.826
$K_0+(K_1-K_0)\sqrt{\alpha}$	-1.361	-0.857	-0.378	0.218	0.759	1.504	2.252	3.156	3.928

Edge moments

Symmetrical	$-b$	$-3b/4$	$-b/2$	$-b/4$	0	$b/4$	$b/2$	$3b/4$	b
φ_0	3,125	1,060	-390	-1,255	-1,540	-1,255	-390	1,060	$3{,}125 \times 10^{-4}$
φ_1	2,190	1,050	365	-20	-140	-20	365	1,050	$2{,}190 \times 10^{-4}$
$\varphi_0+(\varphi_1-\varphi_0)\sqrt{\alpha}$	3,001	1,059	-290	-1,091	-1,354	-1,091	-290	1,059	$3{,}001 \times 10^{-4}$

Asymmetrical

φ_0'	-12,880	-8,974	-5,628	-2,704	0	2,704	5,628	8,874	$12{,}880^{-4}$
φ_1'	-3,400	-2,040	-1,140	-520	0	520	1,140	2,040	$3{,}400^{-4}$
$\varphi_0'+(\varphi_1'-\varphi_0')\sqrt{\alpha}$	-11,619	-8,052	-5,031	-2,414	0	2,414	5,031	8,052	$11{,}619^{-4}$

$$\frac{16\,a^4}{\pi^4 \rho_P\, 2\,b\,a} = 177.44/E; \qquad \frac{16\,a^4}{\pi^4 \rho_P\, 2\,b} = 1580.20/E; \qquad \frac{b^2}{\rho_E} = 1231.46/E$$

Table 8. Slope Coefficients and "Mean" Factors for Beam and Slab Bridge

Applied load at b/6

Slope at b

	Load at		
	0	$b/4$	$b/6$
$K_0' 10^4$	−475	+540	
$\lambda K_0' 10^4$	−158	+360	202
$K_1' 10^4$	−40	+150	
$\lambda K_1' 10^4$	−13	+100	87
$K_\alpha' 10^4 = 202 + (87 - 202)\sqrt{\alpha} = 187$			

Weighting factor, λ, is 0.33 for load at 0 and 0.67 for load at $b/4$.

Slope at $-b$

	Load at		
	0	$+b/4$	$+b/6$
$K_0' 10^4$	−475	−1,310	
$\lambda K_0' 10^4$	−158	−873	−1,031
$K_1' 10^4$	−40	−325	
$\lambda K_1' 10^4$	−13	−217	−230
$K_\alpha' 10^4 = -1{,}031 + (-230 + 1{,}031)\sqrt{\alpha} = -924$			

Shear force

Slope at b

$K_1' = 5{,}200 \times 10^{-4}$; $K_2' = 1{,}705 \times 10^{-4}$; $10^4 K_\alpha' = 5{,}200 + (1{,}705 - 5{,}200)\sqrt{\alpha} = 4{,}735$.

Slope at $-b$

$K_1' = 3{,}440 \times 10^{-4}$; $K_2' = 350 \times 10^{-4}$; $10^4 K_\alpha' = 3{,}440 + (350 - 3{,}440)\sqrt{\alpha} = 3{,}029$.

Edge moments

Symmetrical

Slope at b

$\gamma_0 = 950 \times 10^{-3}$; $\gamma_1 = 584 \times 10^{-3}$; $\gamma_\alpha = 900 \times 10^{-3}$

Slope at $-b$

$\gamma_0 = -950 \times 10^{-3}$; $\gamma_1 = -584 \times 10^{-3}$; $\gamma_\alpha = -900 \times 10^{-3}$

Asymmetrical

Slope at b

$\gamma_1' = 1{,}686 \times 10^{-3}$; $\gamma_2' = 648 \times 10^{-3}$; $\gamma_\alpha' = 1{,}548 \times 10^{-3}$

Slope at $-b$

$\gamma_1' = 1{,}686 \times 10^{-3}$; $\gamma_2' = 648 \times 10^{-3}$; $\gamma_\alpha' = 1{,}548 \times 10^{-3}$

$\frac{H_1 a^2}{\sqrt{\rho_P \rho_E}} = \frac{P a}{\sqrt{\rho_P \rho_E}} = 223.15 \frac{P}{E}$; $\frac{F a^2}{\sqrt{\rho_P \rho_E}} = 1{,}987.21 \frac{F}{E}$; $\frac{b}{\rho_E} = \frac{205.24}{E}$; $\frac{1}{C}\left(\frac{2a}{\pi}\right)^2 = 7{,}916.60$.

For these edge shear forces and moments and the applied load the deflexion profiles are given in table 9 and are compared with the experimental results. Comparing the theoretical results in which the edge moments are considered with those in which the edge moments are ignored, it will be seen that, as in the previous example, the effect of the edge moments is very small and can be neglected. If this is done the derivation of the compatibility equations depends only on the normal distribution coefficients K and the solution is quickly obtained.

Table 9. Theoretical and Experimental Deflexion Profiles for Beam and Slab Bridge With and Without Edge-Stiffening Beams

Position on section	Deflexions in 0.0001 in. due to				
	P	Experimental	$P+F$	$P+F+M$	Experimental
$-b$	10.46	10.00	8.15	7.88	6.30
$-3b/4$	14.49	12.50	11.58	11.40	10.20
$-b/2$	19.56	17.00	16.45	16.34	15.50
$-b/4$	24.75	21.70	20.58	20.53	21.50
0	28.55	27.60	23.57	23.57	23.50
$b/4$	30.30	31.00	23.15	23.20	24.30
$b/2$	30.71	31.50	21.51	21.62	21.00
$3b/4$	31.54	29.30	19.35	19.53	19.00
b	32.00	27.80	17.45	17.70	17.40

The agreement between the theoretical and experimental deflexions is very good and confirms the validity of the analysis when applied to bridges with a torsional parameter not equal to unity.

The distribution of longitudinal bending moments would be found by replacing the factor $\frac{16a^4}{\pi^4 \rho_P 2b}$ by the factor $\frac{4a^2}{\pi^2 2b}$ in the deflexion calculations.

The transverse bending moments would be found in the same way as in the previous example but this time using the interpolation equation

$$M_{y_\alpha} = M_{y_0} + (M_{y_1} - M_{y_0}) \sqrt{\alpha}.$$

The ratio of the flexural stiffness per inch width of the edge beam to the flexural stiffness per inch run of the slab was 11.9 and the ratio of the torsional stiffness per inch width of the edge beam to the torsional stiffness of the slab per inch run was 19.6. The last ratio is much greater than the ratio of 0.5 for the slab bridge but the ratio of the flexural to the torsional stiffness of the edge beam is 41 which is also considerably greater than the limiting value of 5 mentioned previously, indicating that the edge moments can be ignored.

Eccentric Transverse Prestress in Bridges

An analysis of the transverse bending moments in a bridge shows that the value of the maximum possible sagging moment on any transverse section considerably exceeds the maximum possible hogging moment, the one being only about 10% of the other. This being so, there can be no economy in applying a uniform transverse prestress to resist these moments as the applied force must be sufficient to induce a stress equal to the maximum sagging stress at all points on the cross-section of the cross-connexion which often necessitates close spacing of the transverse prestressing tendons. The situation can be relieved by placing the tendons eccentrically so that the maximum possible compressive stress is induced in the bottom face of the cross-connexion without causing unnecessarily high stresses elsewhere on the section. Thus, the required prestressing force is reduced and an increase in the spacing of the prestressing tendons is possible. The maximum allowable eccentricity of the tendons should be such that no tensile stresses are caused in the upper face of the cross-connexion. Then the tensile stresses induced by the live load hogging moments will not exceed 100 lb./in^2 and will normally be less.

The practical difficulties which exist in placing a transverse cable with a curved profile will always make a straight cable more economical. Therefore, in considering the effects of eccentric transverse prestress a straight cable of constant eccentricity e_0 will be assumed without exception.

Since a straight cable induces no vertical reactions anywhere along its length a transversely prestressed bridge can be assumed to be acted upon by equal moments $M_0 \sin \frac{\pi x}{2a}$ along each edge where the value of M_0 depends upon the longitudinal disposition of the prestressing force and upon its eccentricity. To the stresses caused by these bending moments must be added the normal stresses $\frac{P}{A}$, P being the value of the prestressing force.

The effect of the edge moment $M_0 \sin \frac{\pi x}{2a}$ at points across the transverse section can be directly assessed as shown in section 2 (a) by using the curves given in figs. 4 and 5, and the interpolation formula quoted. Thus for any bridge the transverse moment due to eccentric prestress may be expressed in the form

$$M_y = \psi M_0 \sin \frac{\pi x}{2a},$$

where ψ is a coefficient dependent on θ, α, and the point in the transverse section at which the moment is required.

The value of M_0, the effective sinusoidal edge moment, depends on the disposition of the transverse cables. The expressions for M_0 for a number of common dispositions of edge moments, i. e. spacing of transverse cables for a constant prestressing force and eccentricity, are given in fig. 22. It is sufficiently

accurate to take only the first term of these series into consideration. The moments caused by edge moments are then equal to $\psi_\alpha M_0 \sin\frac{\pi x}{2a}$ and M_0 is defined in terms of the actual applied moment per unit length, M. The actual transverse moments caused by live loading will have been determined by means of the μ-coefficient analysis (2) and the stresses due to these moments can be equated to the stresses due to the moments $\psi_\alpha M_0 \sin\frac{\pi x}{2a}$ plus the uniform stress due to prestress $\frac{P}{A}$.

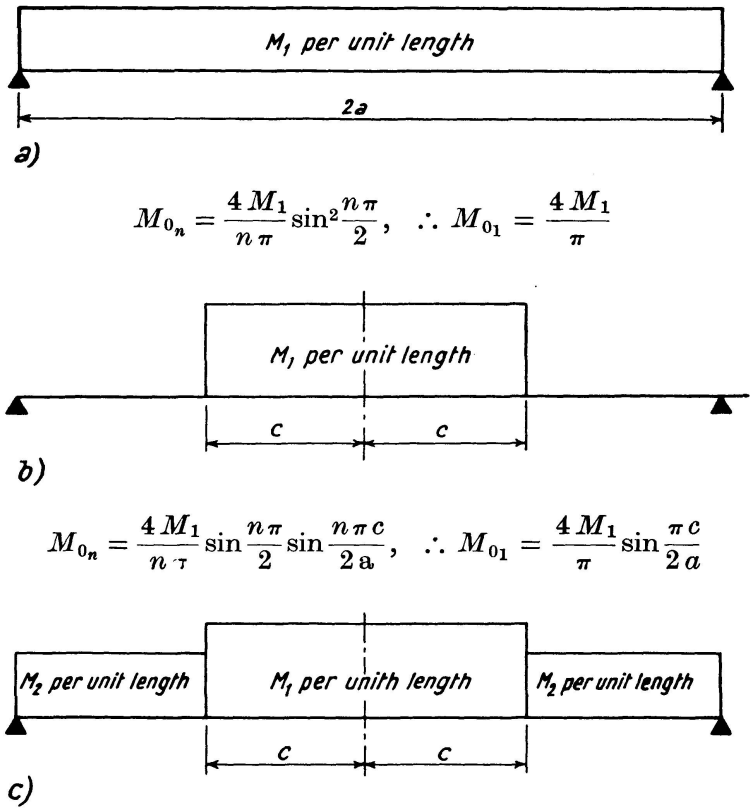

$$M_{0_n} = \frac{4M_1}{n\pi}\sin^2\frac{n\pi}{2}, \quad \therefore M_{0_1} = \frac{4M_1}{\pi}$$

$$M_{0_n} = \frac{4M_1}{n\pi}\sin\frac{n\pi}{2}\sin\frac{n\pi c}{2a}, \quad \therefore M_{0_1} = \frac{4M_1}{\pi}\sin\frac{\pi c}{2a}$$

$$M_{0_n} = \frac{4}{n\pi}\left[(M_1 - M_2)\sin\frac{n\pi}{2}\sin\frac{n\pi c}{2a} + M_2\sin^2\frac{n\pi}{2}\right]$$

$$M_{0_1} = \frac{4}{\pi}\left[(M_1 - M_2)\sin\frac{\pi c}{2a} + M_2\right]$$

Fig. 22. Expressions for M_0 for various longitudinal dispositions of transverse prestress.

Conclusions

It has been shown that the theoretical determination of the effects of edge-stiffening beams gives values which agree with experimental results.

It appears that the effects of the edge moments can be ignored in relation to the effects of edge shear if the ratio of the flexural to the torsional stiffness

of the edge beams is greater than 5, provided that the flexural stiffness per inch width of the edge beam is not considerably greater than the flexural stiffness per inch run of the deck. In the first case examined the ratio of the flexural stiffness per inch width of the edge beam to that of the deck was 6; in the second it was 12; and by studying the magnitude of the effects of the edge moments in these cases a basis is obtained for assessing their possible importance in other bridges. The two structures investigated had quite different values of the parameter α and, therefore, a large range of bridge construction has been covered. The two values of θ were also appreciably different.

The modifying effects of edge shear and edge moments have been found to be less for transverse moments than for the longitudinal effects. For the slab bridge a reduction of 23% was noted in the maximum longitudinal moment with an increase of less than 4% in the maximum transverse moment.

It is often possible therefore, to ignore the modifying effects of the edge forces on the maximum transverse moments. A study of the stiffness ratios given in the text and the accompanying modifying effects will give a basis for deciding whether the inclusion of the edge effects are necessary in the calculation of transverse moments in other bridges.

It should generally be permissible to ignore the effects of edge moment in calculation and the calculation with edge shear alone is almost as simple as the calculation of the load distribution in a uniform bridge. Having once established the equations for the compatibility of edge deflexion for one position of the applied load the equations for other positions follow easily since only the terms involving the applied loads are changed. For all transverse positions of the load the "mean" effects also remain unchanged.

It is, of course, possible in practice to have edge-stiffening beams for which the torsional stiffness is comparable with the flexural stiffness. It is then advisable to include the effects of edge moments. The comprehensive nature of the analysis described still makes the solution possible.

The application of the curves for the coefficient ψ to the determination of the stresses induced by eccentric transverse prestress in bridges shows that there is a rapid decrease from the edge of a bridge to the centre of the transverse section. The bending stresses caused by prestress at the centre of the bridge decrease with increase in the flexural parameter θ. They become zero at a value of θ between 1.1 and 1.2 and there is then no advantage in an eccentric prestress over a uniform prestress. For lower and more practical values of θ the available bending stresses at the centre of the transverse section are greater for small values of the torsional parameter α.

The total stress due to eccentric prestress is the sum of the uniform stress and bending stress produced by edge moments.

As the value of the cable eccentricity is controlled closely by the requirement of no tensile stresses at the edge of the bridge its choice is usually obvious so that the prestressing force P per unit length at various points along the

span can be obtained directly by equating the stresses due to the prestressing force to the maximum stresses caused by the live load on the bridge.

References

1. Morice, P. B. and Little, G., "The analysis of right bridge decks subjected to abnormal loading." London, Cement and Concrete Association, July 1956, pp. 43. Db. 11.
2. Morice, P. B., Little, G. and Rowe, R. E., "Design curves for the effects of concentrated loads on concrete bridge decks." London, Cement and Concrete Association, June 1956, pp. 24. Db. 11a.
3. Morice, P. B. and Little, G., "Load distribution in prestressed concrete bridge systems." The Structural Engineer. Vol. 32, No. 3. March 1954, pp. 83—111. Discussion Vol. 33, No. 1. January 1955, pp. 21—34. C and C A Reprint No. 1.
4. Massonnet, C., "Méthode de calcul des ponts à poutres multiples tenant compte de leur résistance à la torsion". Zürich, International Association for Bridge and Structural Engineering, 1950. Publications Vol. 10, pp. 147—182.
5. Little, G. and Rowe, R. E., "The effect of edge-stiffening beams on bridges." London, Cement and Concrete Association, February 1956, pp. 59. Technical Report TRA/221.
6. Rowe, R. E., "A load distribution theory for bridge slabs allowing for the effect of Poisson's ratio. Magazine of Concrete Research". Vol. 7, No. 20. July 1955, pp. 69—78. C and C A Reprint No. 10.

Summary

A method of calculating the effects of edge-stiffening beams on bridge structures is presented which is used in conjunction with the normal load distribution theories. The theoretical analysis is given in detail elsewhere [5] so only the governing equations for the various effects are given.

The method presented is only applicable where the effective depth of the bridge is constant between the stiffening beams. Where the effective stiffness is considerably reduced at the footpaths or the structural connexion between the parapet beams and the roadway is poor, the modifying effects of the parapet beams will be much less than those given in the paper and can be ignored.

A full analysis of a slab bridge with edge-stiffening beams is made and the results obtained from tests on a Perspex model of the bridge are compared with those derived theoretically. A similar analysis is made for a beam and slab bridge where the torsional parameter, α, of the unstiffened bridge is less than unity. The results are again compared with values found experimentally.

The degree of accuracy to be expected from the theoretical analysis and the percentage changes in the longitudinal and transverse bending moments due to the effects of edge-stiffening beams are estimated. Part of the analysis for the above problem is applied to the effect of eccentric transverse prestress in bridges. This application of the analysis is illustrated.

Résumé

Pour le calcul des poutres raidisseuses de bordure dans les structures portantes des ponts, les auteurs indiquent une méthode qui est employée conjointement avec les méthodes courantes de répartition des charges, L'étude théorique détaillée a été exposée d'autre part (1), de sorte que seules sont indiquées ici les équations relatives aux différentes influences.

Cette méthode ne peut être appliquée que lorsque la hauteur de la structure portante reste constante entre les poutres raidisseuses. Lorsque la rigidité est fortement réduite à l'endroit des trottoirs ou lorsque la liaison constructive entre les poutres de bordure et le tablier est faible, l'influence des poutres de bordure est beaucoup moins grande qu'il n'est admis ici et elle peut être négligée.

Le calcul complet d'un pont dalle avec poutres raidisseuses de bordure est comparé avec les résultats d'une mesure effectuée sur un modèle en Perspex.

Une investigation analogue est effectuée pour un pont à dalle raidie dans lequel le coefficient de torsion α du pont non renforcé est inférieur à l'unité. Les résultats sont ici aussi comparés avec ceux des mesures.

Les auteurs estiment la précision que l'on peut attendre de l'étude théorique ainsi que la variation en pourcentage des moments fléchissants longitudinaux et transversaux, du fait de la présence des poutres raidisseuses de bordure. Une partie de l'étude du problème ci-dessus est appliquée à l'influence d'une précontrainte transversale excentrique. Cette dernière application fait l'objet d'illustrations.

Zusammenfassung

Für die Berechnung von Randversteifungsträgern bei Brückentragwerken wird hier eine Methode angegeben, die in Verbindung mit den übrigen Lastverteilungstheorien angewendet wird. Die detaillierte, theoretische Untersuchung wurde anderswo (1) entwickelt, so daß hier nur die Gleichungen für die verschiedenen Wirkungen angegeben werden.

Diese Methode ist nur dort anwendbar, wo die Brückenstärke zwischen den aussteifenden Trägern konstant bleibt. Wenn die vorhandene Steifigkeit bei den Gehsteigen stark reduziert wird oder auch wenn die konstruktive Verbindung zwischen den Randträgern und der Fahrbahn schwach ist, dann ist der Einfluß der Randträger viel kleiner als in dieser Abhandlung angenommen wurde und kann vernachlässigt werden.

Die komplette Durchrechnung einer Plattenbrücke mit Randversteifungsträgern wird mit den Resultaten einer Messung an einem Perspex-Modell verglichen.

Eine ähnliche Untersuchung wird für eine Plattenbalkenbrücke durchge-

führt, wo der Verdrehungskoeffizient α der unversteiften Brücke kleiner als 1 ist. Wiederum sind die Ergebnisse mit Messungen verglichen.

Weiterhin wird die Genauigkeit, die von der theoretischen Untersuchung zu erwarten ist, und die prozentuale Veränderung der Längs- und Querbiegungsmomente infolge der Randversteifungsträger abgeschätzt. Ein Teil der Untersuchung des obigen Problems wird auf die Wirkungen einer exzentrischen Quervorspannung angewendet. Diese letzte Anwendung ist illustriert.